JOURNAL OF MATERIALS SCIENCE 29 (1994) 404–411

Structure and morphology of titanium nitride films deposited by laser-induced chemical vapour deposition

A.J. SILVESTRE, O. CONDE
Departamento de Física, Universidade de Lisboa, Campo Grande, Ed. CI, 1700 Lisboa, Portugal

R.VILAR
Departamento de Engenharia de Materiais, Instituto Superior Técnico, Av. Rovisco Pais, 1096 Lisboa Codex, Portugal

M.JEANDIN
Ecole des Mines de Paris, Centre des Matériaux P. M. Fourt, B. P. 87, 91003 Evry Cédex, France

Results on the deposition of titanium nitride on AISI M2 tool steel-type substrates by pyrolytic laser chemical vapour deposition are reported. Spots of TiN were deposited from a gas mixture of $TiCl_4$, nitrogen and hydrogen using a continuous wave quasi-TEM_{00} CO_2 laser beam. The morphology and the structure of the deposited material were investigated by optical microscopy, scanning electron microscopy and X-ray diffraction. The chemical composition was studied with a scanning electron microscope with an energy dispersive spectrometer, and with an electron probe microanalyser. The topography of the coating was analysed with a stylus profilometer and different thickness profiles were measured depending on the laser-power densities and irradiation times. The morphology of the films showed a strong dependence on the laser-power density, interaction time and partial pressure of $TiCl_4$.

1. Introduction

Titanium nitride (TiN) belongs to the group IVB transition metal (titanium, zirconium, hafnium) nitrides and has been extensively studied during the last few years [1]. Because of its excellent physical and chemical properties (high melting point, high hardness, low coefficient of friction, low diffusivity and high thermal and electrical conductivities, chemical stability), titanium nitride has been considered a good candidate for a wide variety of technological applications. Beyond their more traditional field of application as protective coatings against wear and corrosion, titanium nitride coatings have also been used as optical coatings [2, 3], in low-resistivity contacts [4] and as diffusion barrier layers for very large-scale integration metallization in silicon device technology [5, 6]. In addition, because of its attractive gold colour, titanium nitride is also very often used in decorative finishes.

Thin films and coatings of TiN have commonly been deposited by various physical vapour deposition (PVD) and chemical vapour deposition (CVD) methods [7]. However, for localized surface protection, as required in electronic or micromechanical applications, it is more advantageous to use a deposition technique that can lead to the desired small-size deposit in a single step. Laser-induced chemical vapour deposition (LCVD) is a selective-area deposition process that has been extensively employed to deposit a wide variety of materials useful in microelectronics [8, 9].

A few studies involving the use of LCVD for depositing titanium nitride films have been previously reported by the authors [10, 11] and by Hopfe *et al.* [12]. Thermodynamic calculations by Knights [13] showed that TiN can act as a protective interlayer between amorphous silica or amorphous alumina coatings and several underlying alloys, in particular Incoloy 800H. The deposition of TiN on substrates of this high-temperature material was investigated earlier and the results summarized in previous papers [10, 11]. The aim of the present work was to deposit hard coatings of titanium nitride on high-speed steels for cutting tools application.

2. Experimental procedure

The deposition system, shown schematically in Fig. 1, consists of a stainless steel vacuum chamber, a high vacuum pumping system based on a cryogenic pump, a reactant gas supply system and a continuous wave CO_2 laser operating dominantly in the TEM_{00} mode [10].

The infrared laser radiation is incident on the substrate at normal angle and the power density is controlled by varying the laser output power, P_l, and by

0022–2461

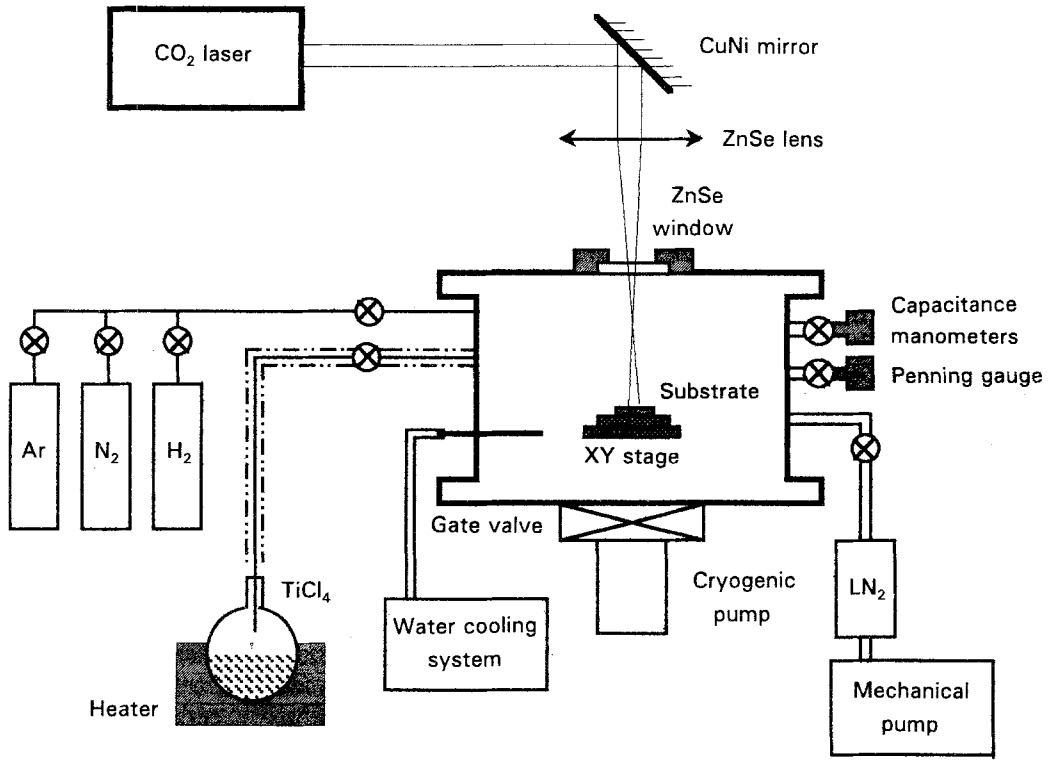

Figure 1 Schematic illustration of the laser chemical vapour deposition (LCVD) system.

modifying the position of the focal point with respect to the surface of the samples. The results reported here were obtained for P_l in the range 500–700 W, with the beam focused either 17 or 30 mm above the substrate surface. Owing to its small divergence, it can be assumed that the beam is focused on the focal plane of the positive ZnSe lens and the laser spot diameter at the substrate surface, d_s (at $1/e^2$ of maximum intensity), could be estimated as 0.9 or 1.6 mm, respectively, using Equation (5) in [14]. Thus, the power density or irradiance, I, which is given by

$$I = (1 - e^{-2}) \frac{4P_l}{\pi d_s^2} \quad (1)$$

took values in the range $(2–10) \times 10^4$ W cm^{-2}. In this study the laser irradiation times were varied from 0.5–10 s.

The experiments were conducted in a closed chamber. Prior to any deposition experiment, the chamber was evacuated to a base pressure of 5×10^{-6} torr (1 torr = 1.333×10^2 Pa) and then filled with titanium tetrachloride, nitrogen and hydrogen at a total pressure of 207 torr. The titanium tetrachloride ($TiCl_4$) is liquid at room temperature. In order to provide sufficient vapour pressure, its container and pipework were heated to 55 °C resulting in a vapour pressure of 52 torr. Then the vapour was pumped into the reaction chamber through a needle valve, and the working vapour pressure of $TiCl_4$ was controlled by a variable temperature finger located inside the reactor and measured with a capacitance manometer. Two different partial pressures of $TiCl_4$ were used, 7 and 10 torr, with the partial pressure ratio $p(N_2)/p(H_2)$ of N_2 to H_2 being kept constant at 1 in all the experiments.

The steel used in this study was a commercially available AISI M2 tool steel, with a spheroidized microstructure resulting from an annealing treatment. Its chemical composition (wt %) was 0.97 C, 0.21 Mn, 4.90 Mo, 3.88 Cr, 1.67 V, 0.22 Si, 0.07 S, 0.03 P, 6.40 W, balance Fe. Cylindrical samples 1 cm high, transversely cut from a 2 cm diameter bar, were used as substrates. The specimens were conventionally heat treated by austenitizing for 5 min at 1220 °C, quenching in oil and then tempering three times at 550 °C for 2 h. After the heat treatment, the samples were ground with metallographic SiC paper to 220 grit finish and cleaned in an ultrasonic bath of acetone. They were then mounted on a X–Y stainless steel motorized table located inside the deposition chamber.

After deposition, the topography of the surface was studied with a Hommel T2-2 stylus profilometer and the microstructure of the films observed without any previous preparation by optical microscopy and scanning electron microscopy (SEM), using both secondary and backscattered electrons. The films were also observed on polished transverse cross-sections of the samples by scanning electron microscopy. Qualitative and semiquantitative chemical microanalysis was performed on some films with an energy dispersive spectrometer (EDS). Furthermore, X-ray image maps were recorded with an automated SX50 CAMECA electron probe microanalyser (EPMA) to evaluate the distribution of selected elements across the surface of the samples. X-ray diffraction was performed with a powder diffractometer using CuK_α radiation.

3. Results

Fig. 2 shows the general appearance of the TiN spots deposited by LCVD from a reactive atmosphere consisting of $TiCl_4$, nitrogen and hydrogen, with a

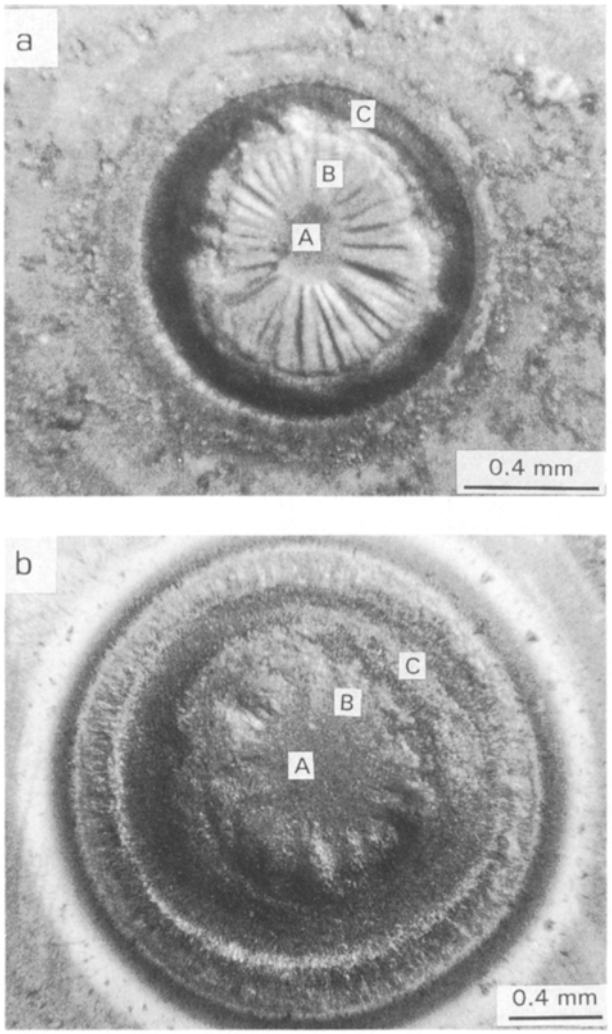

Figure 2 Optical micrographs of the CO_2 laser-induced deposition of titanium nitride on M2 tool steel substrate. Processing conditions: $p(TiCl_4) = 7$ torr; (a) $I = 6.7 \times 10^4$ W cm^{-2} and $t = 6$ s, (b) $I = 2.7 \times 10^4$ W cm^{-2} and $t = 8$ s.

stationary CO_2 laser beam. In Fig. 2a the film deposition lasted for 6 s and was carried out under a laser-power density of 6.7×10^4 W cm^{-2}. Several concentric regions indicated by A, B, C, with different colours and morphologies may be observed on going from the centre to the periphery of the spots. Whenever a relatively high laser-power density was used to induce film deposition, just as in the previous case, a radially corrugated region appears which overlaps the zone marked B in the spots. This zone becomes smoother at shorter interaction times or when the laser irradiance is lower, as in Fig. 2b. Both A and B zones are gold-coloured while the border of the spots (zone C) is usually blue, sometimes appearing as bluish black. The changes of morphology and colour from the centre to the periphery are associated to the radial temperature distribution, and to different chemical reactions at the substrate surface, induced by the quasi gaussian energy profile of the laser beam.

The topography of the surface of the films is also strongly influenced by the laser processing parameters. In fact, three types of profile were obtained depending on the laser-power density and irradiation time. In Fig. 3, four thickness profiles are represented, which were measured on spots deposited at two different values of the laser irradiance, 2.7×10^4 and 6.7×10^4 W cm^{-2}, for different interaction times. As can be seen from the figure, when low power densities were used ($\leqslant 2.7 \times 10^4$ W cm^{-2}), the spots show a broad gaussian type profile, even for the longest interaction time considered (Fig. 3a and b). Otherwise, the thickness profiles show a central depression associated with the well-known volcano-like shape [15–17] (Fig. 3c). In the limiting case of high power densities and long interaction times, melting of the film/substrate, as a whole, can occur at the centre of the deposits (Fig. 3d). In addition, it should be noted that all the profiles show a lack of material in the peripheral region of the spots suggesting that etching of the substrate has occurred.

In order to illustrate the typical structures found in the films, an example is given in Fig. 4 where the scanning electron micrographs show the microstructures developed in the different regions of the spots deposited at 6.7×10^4 W cm^{-2}. The central zone A is always formed by cube-shaped crystals with a mean edge of a few tenths of a micrometre (Fig. 4a). The microstructure of the radially corrugated region B (Fig. 4b) consists of juxtaposed platelets whose mean size varies between 0.2 and 2.2 μm for the interaction times considered here (between 0.5 and 10 s, respectively). The peripheral zone C is usually characterized by a fine granular structure as shown in Fig. 4d. However, in a few cases, a columnar microstructure, where the main growth axis is radially oriented, making a small angle with the substrate surface (Fig. 4c), could be observed in this region.

The micrograph in Fig. 5 shows the cross-section of zone B, after a final polishing with 1 μm diamond paste, of a deposit obtained at the same irradiance as above and with an interaction time of 6 s. It can be seen from this figure that the film is very dense with good adherence and no visible spallation.

As mentioned in Section 2, we have carried out qualitative chemical analysis both with EDS microanalysis and EPMA. Results of EDS analysis at the A and B zones show an intense titanium peak, particularly when the stationary electron beam was concentrated on one of the cubic shaped crystals of zone A (Fig. 6). Similarly, an intense titanium peak was observed when the EDS microanalysis was performed at half the thickness of the cross-sections of the deposits. X-ray image maps were performed in order to study the spatial distribution of selected elements at the top of the coatings. We chose titanium and iron as reference elements. Nitrogen was not considered because its analysis by EPMA is very complex owing to the superposition of the Ti L_1 line at 3.14 nm with the nitrogen K_α emission at 3.16 nm. We also were particularly interested in detecting the presence of elements such as chlorine and oxygen in order to know about possible contaminants in the films. The typical distributions of the four selected elements are illustrated in Fig. 7 for a spot deposited at a power density of 2.7×10^4 W cm^{-2} and an interaction time of 8 s. It can be seen that zone B contains the strongest titanium signal, while this element is absent from the outer rim

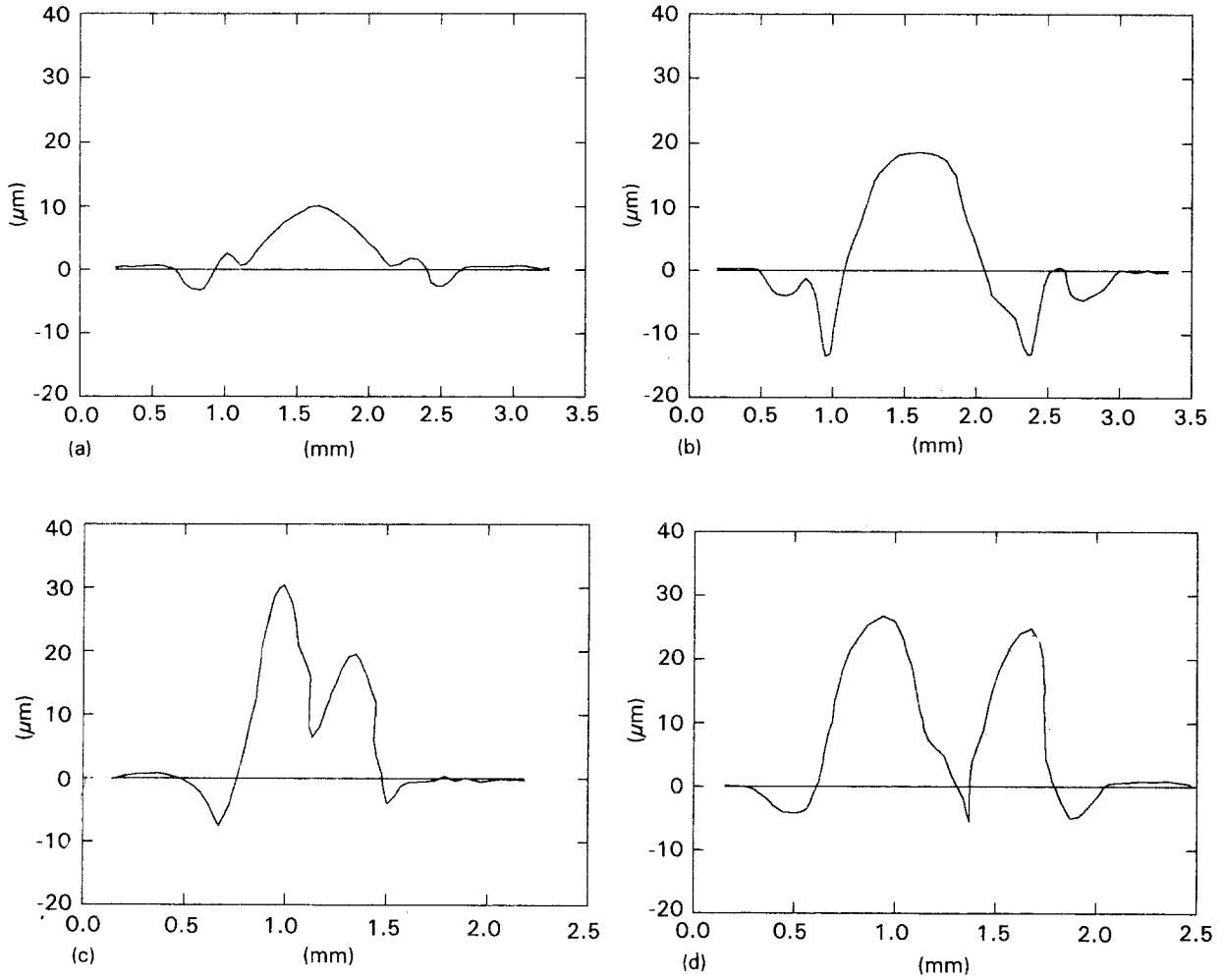

Figure 3 Thickness profiles of LCVD TiN spots deposited on to AISI M2 steel at various laser-power densities and interaction times. (a) $I = 2.7 \times 10^4$ W cm^{-2}, $t_{int} = 2$ s; (b) $I = 2.7 \times 10^4$ W cm^{-2}, $t_{int} = 8$ s; (c) $I = 6.7 \times 10^4$ W cm^{-2}, $t_{int} = 6$ s; (d) $I = 6.7 \times 10^4$ W cm^{-2}, $t_{int} = 10$ s.

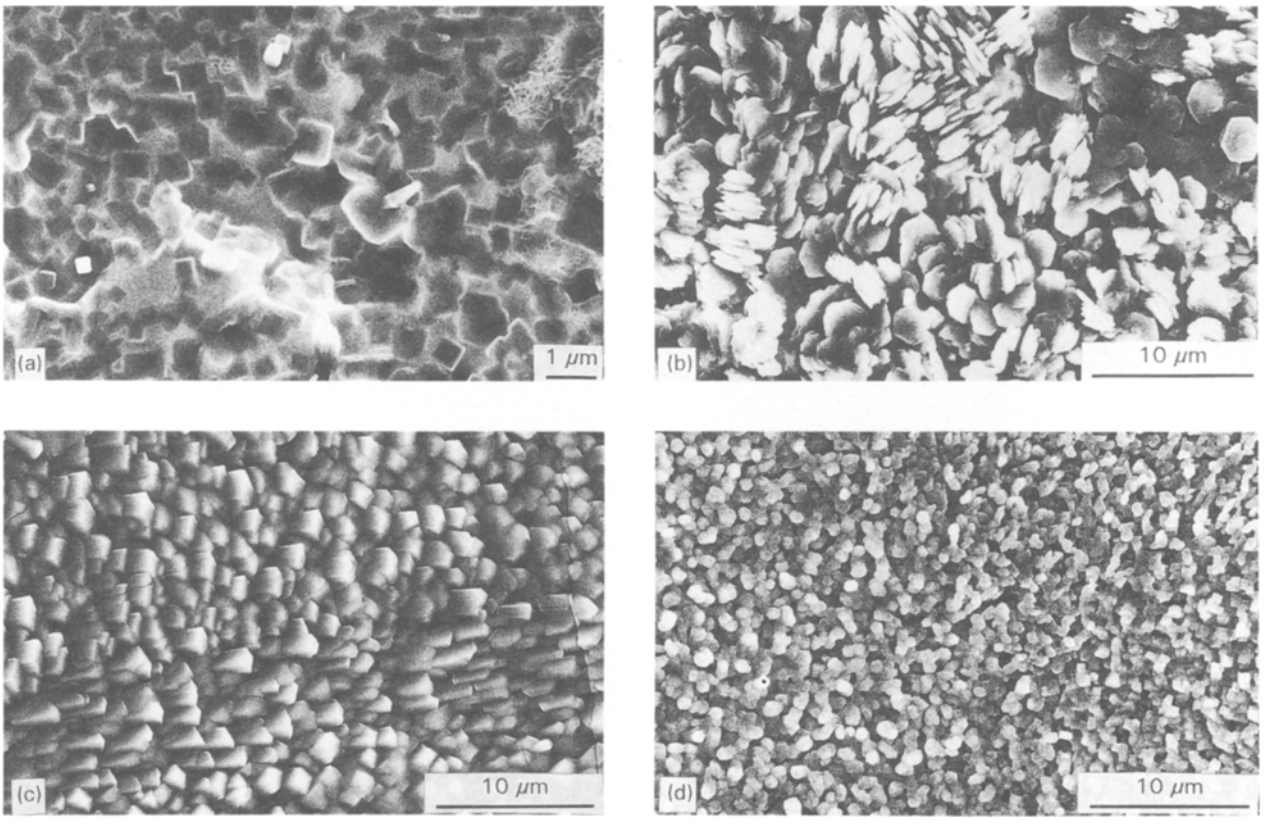

Figure 4 SEM image of (a) zone A, (b) zone B and (c, d) zone C of TiN deposits grown at 6.7×10^4 W cm^{-2} for (a–c) 10 s or (d) 4 s.

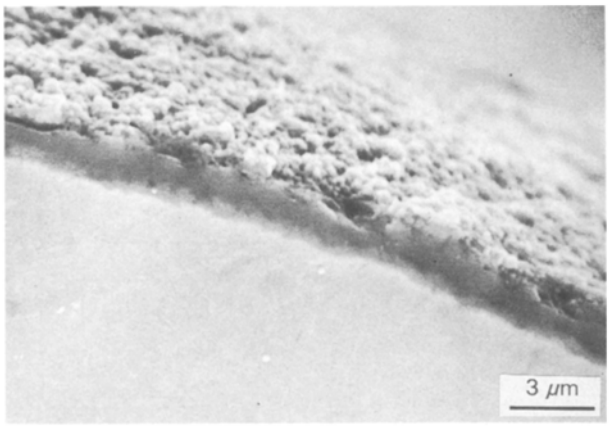

Figure 5 Scanning secondary electron micrograph of a cross-section of LCVD TiN-coated AISI M2 at a laser-power density of 6.7×10^4 W cm^{-2} for 6 s.

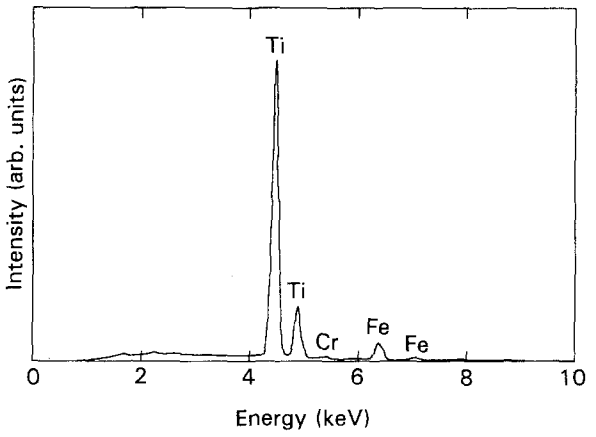

Figure 6 EDS microanalysis performed on the centre of the spot shown in Fig. 2b.

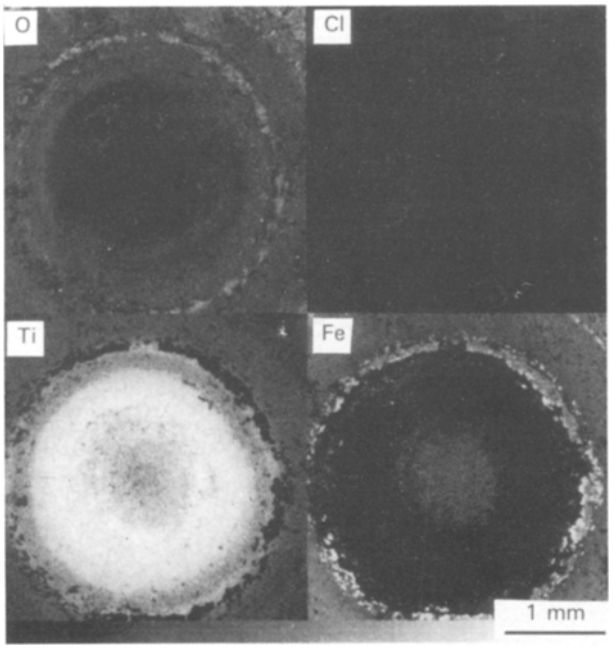

Figure 7 X-ray image mapping of the O, Cl, Ti and Fe elements for the spot presented in Fig. 2b.

of zone C. Conversely, we observed here considerable amounts of iron and oxygen. The amount of chlorine is negligible.

We have studied the influence of the laser-power density and interaction time on the size of the crystallites. Because they are very small in the central zone, as mentioned previously, this influence is more clearly observed in zone B, compared to the central zone A. Fig 8a–d show how the grain size in zone B changes

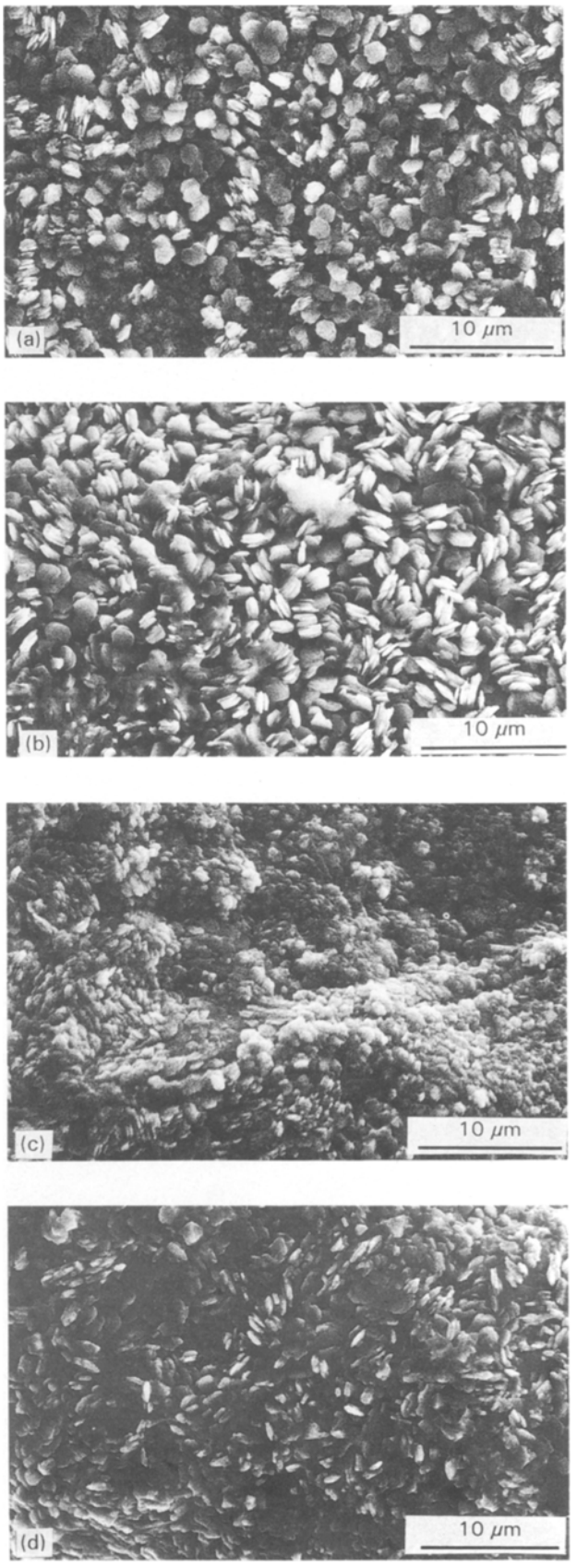

Figure 8 Variation of the crystallites size with deposition parameters. (a) $I = 6.7 \times 10^4$ W cm^{-2}, $t = 6$ s; (b) $I = 6.7 \times 10^4$ W cm^{-2}, $t = 8$ s; (c) $I = 9.3 \times 10^4$ W cm^{-2}, $t = 6$ s; (d) $I = 9.3 \times 10^4$ W cm^{-2}, $t = 8$ s.

with the processing parameters. It can be seen that for a given value of laser irradiance the crystallites are bigger for longer irradiations (a→b, c→d). Conversely, they are smaller when the films are deposited at higher laser-power density keeping the interaction time constant (a→c, b→d). Measured values of the mean grain size as a function of the interaction time are plotted in Fig. 9 for two different values of laser irradiance. We have also investigated the grain-size dependence on the partial pressure of the $TiCl_4$ precursor. As depicted in Fig. 10, the TiN crystal size decreases when the partial pressure of $TiCl_4$ increases.

X-ray diffraction was also carried out on several samples. In spite of the small amount of deposited material, the small size of the spots and the many carbides present in the substrate, there are features in the X-ray diffraction spectra that lead to the conclusion that the films consist of crystalline titanium nitride. In fact, despite their weak intensity, several lines in the experimental diffraction pattern may be observed at the Bragg angles that correspond to the TiN diffraction peaks: (1 1 1), (2 2 0), (3 1 1), (2 2 2) and (4 0 0).

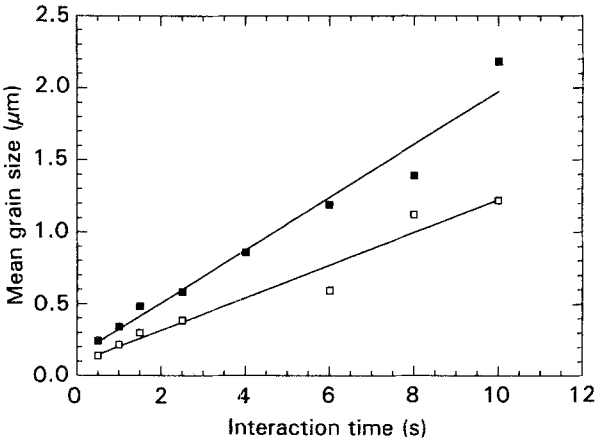

Figure 9 Influence of the interaction time on the size of the crystallites of zone B at two different laser irradiances: (■) 6.7×10^4 W cm^{-2}, (□) 9.3×10^4 W cm^{-2}.

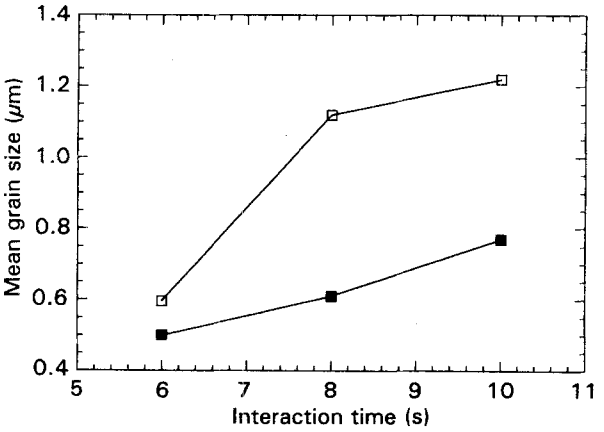

Figure 10 Influence of the partial pressure of $TiCl_4$ on the mean grain size of the films deposited at 9.3×10^4 W cm^{-2}: (□) 7 torr, (■) 10 torr.

4. Discussion

The results of X-ray microanalysis, X-ray diffraction and the golden colour of the films suggest that deposition of TiN was achieved. The topography of the deposited material is important in many applications and the most useful line shape is the flat-topped deposits with rectangular edges. In the LCVD processes this geometry can be achieved with homogenized laser-beam profiles. However, when a gaussian beam is used, sharp edges are difficult to obtain owing to the quasi gaussian surface temperature distribution induced by the laser beam, and leading to an analogous shape of the deposited material. Nevertheless, films with quasi gaussian distribution of thickness can be used as anti-gaussian absorption filters, and therefore may be of great use in optical information processing as pointed out by Xuebiao *et al.* [18]. Increasing the laser irradiance has the effect of increasing temperature at the centre of the laser spot and the thickness profile of the films becomes double-humped. Explanations given to account for this volcano-like shape have been based on high chemical reaction rates, convection from the surface, low sticking coefficients and melting, and even evaporation, at the centre of the heated spots. Of the several theoretical models proposed in order to understand the basic mechanisms of LCVD processes, some of them [16, 19–21] yield deposits with volcanic morphology. Recently, Conde *et al.* [22] applied Kar *et al.*'s model [21] for studying the spatial variation of the thickness of TiN spots deposited on to Incoloy 800H substrates by pyrolytic LCVD with a continuous wave TEM_{00} CO_2 laser beam, and from a reactive atmosphere consisting of $TiCl_4$, nitrogen and hydrogen. Owing to the lack of information on the chemical reaction mechanism and chemical kinetics they assumed that the rate of formation of TiN is first-order on the $TiCl_4$ concentration. The volcanic profile observed under some conditions [11] was reproduced by assuming that the sticking coefficient, γ, of TiN at the substrate surface is temperature dependent. The best agreement with the experimental results was obtained for a linear decrease of γ from 1 to 0 when the temperature increases from 1473 K to 1640 K. In the present work, we can clearly conclude that high power densities should be avoided to prevent the formation of the volcanoes. The non-uniformity of the temperature across the laser-beam diameter and the fact that there exists a steep temperature gradient at the substrate surface may explain not only the topographies described above, but they also suggest that a strong convection can develop in the vapour phase, particularly when the laser irradiance is high, which is responsible for the appearance of the radially corrugated zone in the deposited material.

The microstructures observed in the different zones could be an indication that the deposition regime of the central zone A is different from the deposition regime of the other zones. The central zone corresponds to the highest deposition temperature and the most probable deposition regime is the mass-transport controlled one, which is determined by the balance between the diffusion rate of the various species inside the LCVD chamber and the chemical reaction

rate constant. Probably, the beginning of the radially corrugated zone B marks the end of this regime. The juxtaposed platelets that characterize zone B are highly anisotropic crystals and suggest that the deposition in this zone could be kinetically controlled because plate-like crystals grow in kinetic rather than in diffusion regime [23].

For a given laser-power density, the mean size of the TiN crystallites increases with the interaction time because of the dependence of the growth rate on the maximum temperature attained, which increases with irradiation time. Conversely, it can be seen from Fig. 9 that increasing the laser irradiance from 6.7×10^4 W cm^{-2} to 9.3×10^4 W cm^{-2} decreases the crystal size by a factor of almost 2. Using an instantaneous point-source model [24] we estimated that within the range of interaction times studied, the temperatures attained under an irradiance of 6.7×10^4 W cm^{-2} are lower than those attained at 9.3×10^4 W cm^{-2}. Therefore, a possible explanation for our results could be the existence of a maximum on the growth rate as a function of temperature at which the grain-growth rate would start to decrease as the temperature continues to increase [25].

The decrease of the grain size with an increase of the partial pressure of $TiCl_4$ brings out the strong dependence of the nucleation rate of the titanium nitride on the partial pressure of the $TiCl_4$ precursor. As the supersaturation increases, the nucleation rate increases, decreasing the crystal size. This behaviour was also observed by Kim and Chun [26] in the case of TiN films deposited by conventional CVD from a gas mixture analogous to that considered in this study.

The lack of material in the peripheral regions of all spots profiles is not fully understood at present, but it is believed that this is due to secondary chemical reactions that are favoured at low temperatures. We have plotted in Fig. 11 the Gibb's free energy change with temperature for the two reactions shown in the figure and calculated by using data given elsewhere [27, 28]. At low temperatures and in the presence of an iron source, the most probable reaction of TiN formation is the reduction reaction of titanium tetrachloride by the iron, leading to the formation of iron dichloride ($FeCl_2$), Reaction II. This result was put in evidence experimentally by Michalski and Wierzchon [29], who showed that the presence of an iron source in CVD process from a gas mixture of $TiCl_4$, nitrogen and hydrogen is a prerequisite for the synthesis of titanium nitride at temperatures below 950 °C. Therefore, the lack of material that can be observed on the outer regions of the laser-deposited titanium nitride spots can be attributed to the predominance of Reaction II (Fig. 11), yielding the formation of iron dichloride that evaporates when the temperature increases ($\approx$ 1000 °C), resulting in substrate etching. These regions overlap the blue zones mentioned previously. Munster *et al.* [30] reported, for the same chemical system as ours, a blue coloured compound forming between 500 and 600 °C, attributed to an incomplete reduction reaction. They suggested that is could be an impure form of titanium nitrochloride (TiNCl). However, our X-ray image maps show no considerable amount of chlorine that would support this hypothesis. It is more likely that the bluish colour that can be seen in the peripheral regions of the spots is due to the formation of titanium pentoxide (Ti_3O_5), originated from the reaction of titanium with the oxygen present in the residual atmosphere. This oxide is characterized by a bluish black colour and can be stablized at room temperature by a small amount of iron [31].

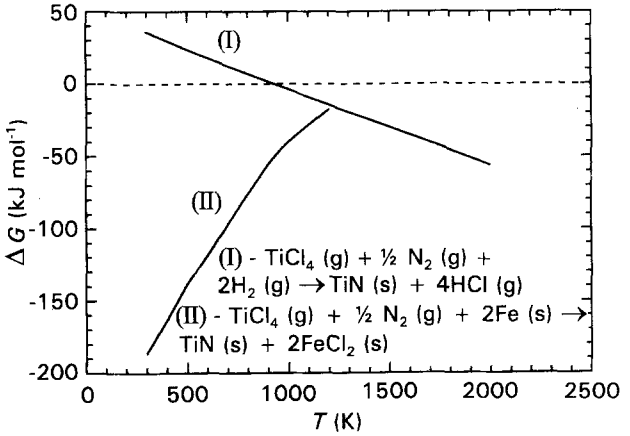

Figure 11 Gibbs' free energy change versus temperature for Reactions I and II.

5. Conclusion

We have shown that deposition of TiN on AISI M2 tool steel substrates may be successfully achieved by pyrolytic LCVD using a continuous wave CO_2 laser.

The deposited spots show several concentric polycrystalline regions characterized by different microstructures. Also, different surface profiles were obtained depending on the laser-power densities and irradiation times. For moderate laser-power densities and interaction times, dense films with good adherence and a quasi gaussian line shape were obtained. If a kinetically controlled deposition is intended and/or the volcano-like effect is to be avoided, then low laser-power densities should be used.

For the laser irradiance and interaction time ranges investigated in this study, a lack of material is shown on the outer rim of the spot profiles, which may be attributed to the formation at lower temperatures of a low iron chloride that evaporates when the temperature increases.

The TiN grain size is an increasing function of the irradiation time and a decreasing function of the partial pressure of the $TiCl_4$ precursor. High power densities can play an important role in the grain-growth rate, limiting the grain growth.

Acknowledgements

The authors gratefully acknowledge the financial support of Junta Nacional de Investigação Científica e Tecnológica, Lisboa, Portugal and of P.S.A. Peugeot Citroen, Vélizy, France. Technical assistance by Mrs. S.L. Fontaine was also very much appreciated.

References

1. J. E. SUNDGREN and H. T. HENTZELL, *J. Vac. Sci. Technol.* **A4** (1986) 2259.
2. E. VALKONEN, T. KARLSSON, B. KARLSSON, and B. O. JOHANSSON, in "Proceedings of the SPIE, Thin Film Technologies" edited by J. R. Jacobsson, Vol. 401 (1983) p.375.
3. K. E. ANDERSSON, M. K. WAHLSTROM and A. ROOS, *Thin Solid Films* **214** (1992) 213.
4. M. OSTLING, S. NYGREN, C. S. PETERSSON, H. NORSTROM, R. BUCHTA, H. O. BLOM and S. BERG, *ibid.* **145** (1986) 81.
5. M. DAPOR, M. ELENA, S. GIRARDI, G. GINUTA, L. GUZMAN and M. NARSALE, *ibid.* **153** (1987) 303.
6. M. MANDL, H. HOFFMANN, and P. KUCHER, *J. Appl. Phys.* **68** (1990) 2127.
7. R. F. BUNSHAH, *J. Vac. Sci. Technol.* **B2** (1984) 789.
8. D. BAUERLE, in "Laser Diagnostics and Photochemical Processing for Semiconductor Devices", Materials Research Society Symposium, Vol.17, edited by R. M. Osgood, S. R. Brueck and H. R. Scholssberg (North-Holland, Amsterdam, 1983) p.19.
9. Y. RYTZ-FROIDEVAUX, R. P. SALATHE and H. H. GILGEN, *Appl. Phys.* **A37** (1985) 121.
10. O. CONDE, J. MARIANO, A. J. SILVESTRE and R. VILAR, in "Proceedings of the 3rd European Conference on Laser Treatment of Materials", ECLAT '90, Erlangen, September 1990, edited by H. W. Bergman and R. Kupfer (Sprechsal, Coburg, 1990) p. 145.
11. O. CONDE, M. L. G. FERREIRA, P. HOCHHOLDINGER, A. J. SILVESTRE and R. VILAR, *Appl. Surf. Sci.* **54** (1992) 130.
12. V. HOPFE, A. TEHEL, A. BAIER and J. SCHARSIG, *ibid.* **54** (1992) 78.
13. C. F. KNIGHTS, AERE Harwell Report HL88/532, Oxfordshire, UK (1988).
14. J. T. LUXON, *Laser Applic.* **3** (10) (1984) 83.
15. S. D. ALLEN, *J. Appl. Phys.* **52** (1981) 6501.
16. I. P. HERMAN, R. A. HYDE, B. M. McWILLIAMS, A. H. WEISBERG and L. L. WOOD, in "Laser Diagnostics and Photochemical Processing for Semiconductor Devices", Materials Research Society Symposium, Vol. 17 edited by R. M. Osgood, S. R. Brueck and H. R, Schlossberg (North-Holland, Amsterdam, 1983) p. 9.
17. C. R. MOYLAN, T. H. BAUM and C. R. JONES, *Appl. Phys.* **A40** (1986) 1.
18. L. XUEBIAO, Z. JIE and Q. MINGXIN, *Thin Solid Films* **196** (1991) 95.
19. S. D. ALLEN, R. Y. JAN, R. H. EDWARDS, S. M. MAZUK and S. D. VERNON, *SPIE* **459** (1984) 42.
20. D. C. SKOUBY and K. F. JENSEN, *J. Appl. Phys.* **63** (1988) 198.
21. A. KAR, M. N. AZER and J. MAZUMDER, *ibid.* **69** (1991) 757.
22. O. CONDE, A. KAR and J. MAZUMDER, *ibid.* **72** (1992) 754.
23. E. J. GIVARGIZOV, "Highly anisotropic crystals" (Reidel, Dordrecht, 1987).
24. H. S. CARLSLAW and J. C. JAEGER, "Conduction of heat in solids", 2nd Edn (Oxford University Press, New York, 1959).
25. E. S. MACHLIN, "An introduction to aspects of thermodynamics and kinetics relevant to materials science" (Gyro Press, New York, 1991) p. 237.
26. M. S. KIM and J. S. CHUN, *Thin Solid Films* **107** (1983) 129.
27. M. W. CHASE, Jr., C. A. DAVIES, J. R. DONEY, Jr., D. J. FRURIP, R. A. McDONALD and A. N. SYVERUD "JANAF Thermochemical Tables", 3rd Edn (American Chemical Society and American Insitute of Physics) *J. Phys. Chem. Ref. Data* **14** Suppl. 1, (1985).
28. I. BARIN, "Thermochemical Data of Pure Substances" (VCH Verlagsgesellschaft, Weinheim, 1989).
29. J. MICHALSKI and T. WIERZCHON, *J. Mater. Sci. Lett.* **8** (1989) 779.
30. Cited by C. F. POWELL, in "Vapour Deposition", edited by C. F. Powell, J. M. Oxley and J. M. Blocher Jr (Wiley, 1966) p. 380.
31. R. J. H. CLARK, "The chemistry of titanium", Pergamon Texts in Inorganic Chemistry, Vol. 19 (Pergamon Press, Oxford, 1975) p. 375.

Received 3 November 1992
and accepted 10 March 1993